

Supernova, Hypernova and Gamma Ray Bursts*

Arnon Dar

Physics Department and Space Research Institute, Technion, Haifa 32000, Israel

the date of receipt and acceptance should be inserted later

Abstract. Recent observations suggest that gamma ray bursts (GRBs) and their afterglows are produced by highly relativistic jets emitted in core collapse supernova explosions (SNe). The result of the event, probably, is not just a compact object plus a spherical ejecta: within days, a fraction of the parent star falls back to produce a thick accretion disk around the compact object. Instabilities in the disk induce sudden collapses with ejection of highly relativistic “cannonballs” of plasma, similar to those ejected by microquasars. The jet of cannonballs exit the supernova shell/ejecta reheated by their collision with it, emitting highly forward-collimated radiation which is Doppler shifted to γ -ray energy. Each cannonball corresponds to an individual pulse in a GRB. They decelerate by sweeping up the ionised interstellar matter in front of them, part of which is accelerated to cosmic-ray energies and emits synchrotron radiation: the afterglow. The Cannonball Model cannot predict the timing sequence of these pulses, but it fares very well in describing the total energy, energy spectrum, and time-dependence of the individual γ -ray pulses and afterglows. It also predicts that GRB pulses are accompanied by detectable short pulses of TeV neutrinos and sub TeV γ -rays, that are much more energetic and begin and peak a little earlier.

Key words: hypernova, supernovae, gamma ray bursts

1. Introduction

Once upon a time, Gamma Ray Bursts (GRBs) constituted a sheer mystery, whose unassailability was reflected in the scores of extremely different ideas proposed to explain them. In spite of giant strides in the recent observations—the discovery of GRB afterglows (Costa et al. 1997; van Paradijs et al. 1998), the discovery of the association of GRBs with supernovae (Galama et al. 1998), and the measurements of the redshifts of their host galaxies (Metzger et al. 1997)—the origin of GRBs is still an enigma. In the recent past, the generally accepted view has been that GRBs are generated by synchrotron emission from fireballs, or firecones, produced by collapse or

merger of compact stars (Paczynski 1986; Goodman et al. 1987; Meszaros and Rees 1992) by failed supernovae or collapsars (Woosley 1993; Woosley and MacFadyen 1999; MacFadyen and Woosley 1999; MacFadyen et al. 1999) or by hypernova explosions (Paczynski 1998).

I have been asked to discuss hypernovae - hypothetical spherical fireballs that are generated by gravitational collapse of very massive stars and generate GRBs. But “I come to bury Caesar not to praise him” (Shakespeare, “Julius Caesar” Act. III Sc.II): Various observations suggest that **most** GRBs are produced by highly collimated ultrarelativistic jets from stellar collapse (Shaviv and Dar 1995; Dar 1998; Dar and Plaga 1999), probably, from supernova explosions (Dar and Plaga 1999; Cen 1999; Woosley et al. 1999; Woosley and MacFadyen 1999; MacFadyen and Woosley 1999; Dar and De Rújula 2000a; Dar and De Rújula 2000b), and not in spherical explosions that convert kinetic energy to GRBs with total γ -ray energy in excess of 10^{54} erg.

In my talk I will review briefly the evidence that GRBs are associated with SNe. Then I will review the Cannonball (CB) Model of GRBs that was recently proposed by Dar and De Rújula (2000a, 2000b) and explains how GRBs are produced in SNe. Its success in describing the total energy, energy spectrum, the time-dependence of the individual γ -ray pulses in GRBs and the GRB afterglows will be demonstrated.

2. The GRB–SNe association

There is mounting evidence for an association of supernova (SN) explosions and GRBs. The first example was GRB 980425 (Soffitta et al. 1998; Kippen 1998), within whose error circle SN1998bw was soon detected optically (Galama et al. 1998) and at radio frequencies (Kulkarni et al. 1998a). The chance probability for a spatial and temporal coincidence is less than 10^{-4} (e.g. Galama et al. 1998), or much smaller if the revised BeppoSAX position (e.g., Pian, 1999) is used in the estimate. The unusual radio (Kulkarni et al. 1998a; Wieringa et al. 1999) and optical (Galama et al. 1998; Iwamoto et al. 1998) properties of SN1998bw, which may have been blended with the

afterglow of GRB 980425, support this association. The exceptionally small fluence and redshift of GRB 980425 make this event very peculiar, a fact that we discuss in detail in section 7.

Evidence for a SN1998bw-like contribution to a GRB afterglow (Dar 1999a) was first found by Bloom et al. (1999) for GRB 980326, but the unknown redshift prevented a quantitative analysis. The afterglow of GRB 970228 (located at redshift $z = 0.695$) appears to be overtaken by a light curve akin to that of SN1998bw (located at $z_{\text{bw}} = 0.0085$), when properly scaled by their differing redshifts (Dar 1999b). Let the energy flux density of SN1998bw be $F_{\text{bw}}[\nu, t]$. For a similar supernova located at z :

$$F[\nu, t] = \frac{1+z}{1+z_{\text{bw}}} \frac{D_L^2(z_{\text{bw}})}{D_L^2(z)} \times F_{\text{bw}} \left[\nu \frac{1+z}{1+z_{\text{bw}}}, t \frac{1+z_{\text{bw}}}{1+z} \right] A(\nu, z), \quad (1)$$

where $A(\nu, z)$ is the extinction along the line of sight. The SN–GRB association in the case of GRB 970228 was re-confirmed by Reichart (1999) and by Galama et al. (2000). Evidence of similar associations is found for GRB 990712 (Hjorth et al. 1999; Sahu et al. 2000), GRB 980703 (Holland 2000) and GRB 000418: an example that we show in Fig. 5. In the case of GRB 990510 the observational evidence (Sokolov et al. 2000) is marginal. For the remaining cases in Table I the observational data preclude a conclusion, for one or more reasons: the late afterglow is not measured; $F_{\text{bw}}[\nu']$ is not known for large $\nu' \simeq \nu(1+z)$; the GRB’s afterglow or the host galaxy are much brighter than the SN. The case of GRB 970508, for which the afterglow in the R band is brighter than a SN contribution given by Eq. (1), is shown in Fig. 6.

All in all, it is quite possible that a good fraction of GRBs are associated with SNe, perhaps even *all* of the most frequent, long-duration GRBs. The converse statement—that most SNe of certain types are associated with GRBs—appears at first sight to be untenable. The rate of Type Ib/Ic/II SNe has been estimated from their observed rate in the local Universe (e.g. Van den Bergh & Tammann 1991) and the star formation rate as function of redshift, to be 10 s^{-1} in the observable Universe (Madau 1998). The observed rate of GRBs is a mere 1000 y^{-1} . Thus, very few of these SNe produce *visible* GRBs. But, if the SN-associated GRBs were beamed within an angle $\theta \sim 3.6 \times 10^{-3}$, only a fraction $\pi \theta^2 / 4\pi \sim 3 \times 10^{-6}$ would be visible, making the observed rates compatible and making possible a rough one-to-one SN–GRB association (or a ten-to-one association for $\theta \sim 1 \times 10^{-2}$).

3. The Cannonball Model of GRBs

3.1. The engine

The ejection of matter in a supernova (SN) explosion is not fully understood. The known mechanisms for impart-

ing the required kinetic energy to the ejecta are inefficient: the theoretical understanding of core-collapse SN events is still unsatisfying. It has been proposed (De Rújula 1987; Dar and Plaga 1999; Cen 1999; Woosley and MacFadyen 1999; Dar and De Rújula 2000a and references therein) that the result of a SN event is not just a compact object plus a spherical ejecta: a fraction of the parent star may be ejected, but another fraction of its mass may fall back onto the newly born compact object. For vanishing angular momentum, the free-fall time of a test-particle from a parent stellar radius R_* onto an object of mass M_c is:

$$t_{\text{fall}} = \pi \left[\frac{R_*^3}{8 G M_c} \right]^{1/2} \sim 1 \text{ day} \left[\frac{R_*}{10^{12} \text{ cm}} \right]^{3/2} \left[\frac{1.4 M_\odot}{M_c} \right]^{1/2}. \quad (2)$$

The free-fall time may be shorter if the mass of the falling material is not small relative to that of the compact object and if the specific angular momentum is small, or much longer if the specific angular momentum is considerably large, as it is in most stars. In both cases it is quite natural to assume that infalling material with non-vanishing angular momentum settles into an orbiting disk, or a thick torus if its mass is comparable to M_c and that, as observed in other cases of significant accretion onto a compact object (microquasars and active galactic nuclei) in which the infalling material is processed in a series of “catastrophic” accretions, jets of relativistic CBs of plasma are ejected (e.g., Belloni et al. 1997; Mirabel and Rodriguez 1999a,b). Their composition is assumed to be “baryonic”, as it is in the jets of SS 433, from which Doppler shifted Ly_α and K_α lines of various elements, such as Fe, Ni, Mg, Si, S and Ar, have been detected (Margon 1984; Kotani et al 1996), although the violence of the relativistic jetting-process should in our case break most nuclei into their constituents.

The cannonball model of GRBs (Dar and De Rújula 2000a,b) is illustrated in Fig. 1. In brief, the CB model is the following. A sequence of highly relativistic cannonballs is emitted during a core-collapse SN. These cannonballs may be emitted right after the initial collapse (Dar and Plaga 1999; Cen 1999; Woosley and MacFadyen 1999; MacFadyen and Woosley 1999; MacFadyen et al. 1999) and hit a massive shell at a typical radius of $R_S \sim 3 \times 10^{15} \text{ cm}$ formed by strong wind emission in the Red Supergiant or variable Blue Giant presupernova phase (for evidence see e.g., Salamanca et al. 1998; Fassia et al. 2000). They may be emitted in a second collapse (De Rújula 1987) at a time t_{fall} of $\mathcal{O}(1)$ day after a SN core-collapse. By this time the SN outer shell, traveling at a velocity $v_S \sim c/10$ (see, e.g., Nakamura et al. 2000) has moved to a distance:

$$R_S = 2.6 \times 10^{14} \text{ cm} \left(\frac{t_{\text{fall}}}{1 \text{ d}} \right) \left(\frac{10 v_S}{c} \right). \quad (3)$$

As it hits a massive shell, the CB slows down and heats up. Its radiation is obscured by the shell up to a distance of order one radiation length from the shell's outer surface. As this point is reached the emitted radiation from the CB which continues to travel, expand and cool down, becomes visible. This radiation, which is boosted and collimated by the ultrarelativistic motion of the CB, and time contracted due to time aberration in the observer frame, appears as a single GRB pulse. The observed duration of a GRB pulse is its radiative cooling time after it becomes visible. The total duration of a GRB with many pulses is the total emission time of CBs with large Doppler factors by the central engine. As the mechanism producing relativistic jets in accretion is not well understood, the CB model is unable to predict the timing sequence of the successive GRB pulses but, the CB model is quite successful in describing the total energy, energy spectrum and time-dependence *within single GRB pulses* (Dar and De Rújula 2000b).

3.2. Relativistic aberration, boosting and collimation

Let $\gamma = 1/\sqrt{1-\beta^2} = E_{\text{CB}}/(M_{\text{CB}}c^2)$ be the Lorentz factor of a CB, that diminishes with time as the CB hits the SN shell and as it subsequently plows through the interstellar medium. Let t_{SN} be the local time in the SN rest system, t_{CB} the time in the CB's rest system and t the time of a stationary observer viewing the CB at redshift z from an angle θ away from its direction of motion. Let x be the distance traveled by the CB in the SN rest system. The relations between the above timings are:

$$dt = \frac{(1+z) dt_{\text{CB}}}{\delta} = \frac{(1+z) dt_{\text{SN}}}{\delta \gamma} = \frac{(1+z) dx}{\beta \gamma \delta c} \quad (4)$$

where the Doppler factor δ is:

$$\delta \equiv \frac{1}{\gamma(1-\beta \cos \theta)} \simeq \frac{2\gamma}{(1+\theta^2\gamma^2)}, \quad (5)$$

and its approximate expression is valid for $\theta \ll 1$ and $\gamma \gg 1$, the domain of interest here. In what follows we will set $t=0$ at the moment when the CB hits the shell. Notice that for large γ and $\theta\gamma \sim 1$, there is an enormous "relativistic aberration": $dt \sim dt_{\text{SN}}/\gamma\delta$ and the observer sees a long CB story as a film in extremely fast motion.

The energy of the photons radiated by a CB in its rest system, E_{CB}^γ and the photon energy, E , measured by a cosmologically distant observer are related by:

$$E = \frac{\delta E_{\text{CB}}^\gamma}{1+z}, \quad (6)$$

with δ as in Eq.(5). If $E_{\text{pulse}}^{\text{rest}}$ is the CB total emitted radiation in its rest frame, an observer at a luminosity distance $D_L(z)$ from the CB that is viewing it at an angle $\theta \ll 1$ from its direction of motion would measure a "total" (time- and energy-integrated) fluence per unit area:

$$\frac{dF}{d\Omega} \simeq \frac{(1+z) E_{\text{pulse}}^{\text{rest}}}{4\pi D_L^2} \delta^3. \quad (7)$$

Only if traveling with a large Lorentz factor $\gamma > 10^2$ at a small angle $\theta \sim 1/\gamma$ relative to the line of sight, will a CB at a cosmological distance be visible.

3.3. Jet energy and CB mass

Let "jet" stand for the ensemble of CBs emitted in one direction in a SN event. If a momentum imbalance between the opposite-direction jets is responsible for the large peculiar velocities $v_{\text{NS}} \approx 450 \pm 90 \text{ km s}^{-1}$ (Lyne and Lorimer 1994) of neutron stars born in SNe, the jet kinetic energy E_{jet} must be, as assumed in the CB model for the GRB engine, larger than $\sim 10^{52}$ erg (e.g. Dar and Plaga 1999). The jet-emitting process may be "up-down" symmetric to a very good approximation, in which case the jet energies may be much bigger. There is evidence that in the accretion of matter by black holes in quasars (Celotti et al. 1997; Ghisellini 2000) and microquasars (Mirabel and Rodriguez 1999a,b) the efficiency for the conversion of gravitational binding energy into jet energy is surprisingly large. If in the production of CBs the central compact object in a SN ingurgitates several solar masses, it is not out of the question that E_{jet} be as large as $M_\odot c^2 \sim 1.8 \times 10^{54}$ erg. A compromise value, 10^{53} ergs, as the reference jet energy was adopted in the CB model of GRBs.

Average GRBs have some five to ten significant pulses, so that the fraction f of the jet energy carried by a single CB may typically be $1/5$ or $1/10$. A value $E_{\text{CB}} = 10^{52}$ erg was adopted as a reference value. For this value, the CB's mass is comparable to an Earth mass: $M_{\text{CB}} \sim 1.8 M_\oplus (10^3/\gamma)$, for a Lorentz factor of $\gamma = \mathcal{O}(10^3)$, that was found by fitting the GRB properties (see later).

3.4. The making of the GRB

The general properties of GRB pulses in the CB model are not sensitive to the complex details of the CB's collision with the shell. They can be estimated from the overall energetics and approximate treatment of the cooling of the CB by radiation and expansion as it reaches the transparent outskirts of the shell.

The density profile of the outer layers of an SN shell as a function of the distance x to the SN center can be inferred from the photometry, spectroscopy and evolution of the SN emissions (see e.g. Nakamura et al. 2000 and references therein). The observations can be fit by a power law, x^{-n} , with $n \sim 4$ to 8 . The results are sensitive to this density profile only in the outer region where the SN shell becomes transparent (and the measurements are made), so that one can adopt the same profile at all $x > R_S$:

$$\rho(x) = \rho(R_S) \Theta(x - R_S) \left[\frac{R_S}{x} \right]^n. \quad (8)$$

The SN-shell grammage still in front of a CB located at x is:

$$X_S(x) = \int_x^\infty \rho(y) dy = \frac{M_S}{4\pi R_S^2} \left[\frac{R_S}{x} \right]^{n-1}, \quad (9)$$

where M_S and R_S are the total mass and radius, respectively, of the shell. For photons in the MeV domain the attenuation length is similar, within a factor 2, in all elements from H to Fe (Groom et al., 2000), and can be roughly approximated by:

$$X_\gamma(E) \sim 1.0 (E/\text{keV})^{0.33} \text{ g cm}^{-2}. \quad (10)$$

The value of $X_\gamma(E)$ in the $E = 10 \text{ keV}$ to 1 MeV domain (2.1 to 9.8 gr/cm^2) is close to the attenuation length in a hydrogenic plasma ($X_\gamma^{\text{ion}} \simeq m_p/\sigma_T \simeq 2.6 \text{ gr/cm}^2$, with m_p the proton's mass and $\sigma_T \simeq 0.65 \times 10^{-24} \text{ cm}^2$ the Thomson cross-section). Therefore, it makes little difference in practice whether or not we take into account that the SN-shell material reached by the CB may be ionized by its previously emitted radiation. The position $X - t_p$ at which the SN shell becomes (one-radiation-length) transparent is then given by :

$$x_{t_p}(E) = R_S \left[\frac{M_S}{4\pi R_S^2} \frac{1}{X_\gamma(E)} \right]^{\frac{1}{n-1}} \propto E^{-0.33/(n-1)}, \quad (11)$$

whose energy dependence is extremely weak. Blue-shifted to the SN rest-system, as in Eq.(6), GRB photons have energies in the MeV range.

In its rest frame, the front surface of the CB is bombarded by the nuclei of the shell, which have an energy $m_p c^2 \gamma \sim 1 \text{ TeV}$ per nucleon, roughly $1/3$ of which (from $\pi^0 \rightarrow \gamma\gamma$ decays) is converted into these γ -rays within $X_p \approx m_p/\sigma_{\text{in}}(\text{pp}) \approx 50 \text{ g cm}^{-2}$, where $\sigma_{\text{in}}(\text{pp})$ is the nucleon-nucleon inelastic cross section. These high energy photons initiate electromagnetic cascades that eventually convert their energy to thermal energy within the CB. The radiation length of high energy γ 's in hydrogenic plasma, dominated by $e^+ e^-$ pair production, is $X_{\gamma_e} \approx 63 \text{ g cm}^{-2}$, comparable to X_p . The radiation length of thermalized photons in a hydrogenic plasma is $X_\gamma^{\text{ion}} \approx m_p/\sigma_T \approx 2.6 \text{ g cm}^{-2}$.

Assume that the quasi-thermal emission rate from the CB, within X_γ^{ion} from its surface, is in dynamical equilibrium with the fraction of energy deposited by the CB's collision with the shell in that outer layer. The temperature of the CB's front is then roughly given by:

$$T(x) \simeq \left[\frac{(n-1) X_\gamma m_p c^3 \gamma^2 \sigma_{\text{in}}(\text{pp})}{6 \sigma_{X_{t_p}} X_{\gamma_e} \sigma_T^2} \right]^{\frac{1}{4}} \left[\frac{x}{x_{t_p}} \right]^{-\frac{n}{4}}, \quad (12)$$

Remarkably, only the Lorentz factor of the CBs when they exit the shell, but neither their mass nor their energy, appear in the above expression, except for the fact that, for the result to be correct, they must be large enough for the CB to pierce the shell and remain relativistic.

The CB temperature at t_{t_p} is not sensitive to the exact value of n , unlike its time dependence. For $n = 8$ and $M_s = 10 M$, the value of x_{t_p} is $\approx 3 R_S$, and for t close to t_{t_p} or later:

$$T(t) \simeq 0.16 \text{ keV} \left[\frac{t_{t_p}}{t} \right]^2 \left[\frac{\gamma(t)}{10^3} \right]^{\frac{1}{2}}. \quad (13)$$

This estimate is valid as long as the surface temperature of the optically thick CB is higher than the internal temperature of the CB that under the assumption of isentropic expansion decreases with time only like $T_{\text{CB}} \sim 1/R_{\text{CB}} \sim 1/t$.

The observed energy and time dependence of the photon intensity (photon number per unit area, N) of a single pulse in a GRB at an angle θ relative to the CB's motion is predicted to be:

$$\frac{dN}{dE dt} \equiv \frac{1+z}{4\pi D_L^2} \delta^2 \frac{dn_\gamma}{dE dt}, \quad (14)$$

$$\frac{dn_\gamma}{dE dt} \simeq \frac{2\pi\sigma}{\zeta(3)} \frac{[R_{\text{CB}}[t] E(1+z)/\delta]^2 \text{Abs}(E, t)}{\text{Exp}\{E(1+z)/(\delta T[t])\} - 1}, \quad (15)$$

with $R_{\text{CB}}[t] \simeq ct/\sqrt{3}\gamma$ and $T[t]$ as in Eq.(12), and where

$$\text{Abs}(E, t) = \text{Exp} \left[-\frac{X_S(x[t])}{X_\gamma(E(1+z))} \right] \quad (16)$$

is the attenuation of the flux in the shell.

The mean photon energy of a black body radiation is approximately $2.7 T$. Thus, around peak energy flux, the mean energy of the observed photons is

$$\langle E_\gamma \rangle \simeq \frac{0.45}{1+z} \left[\frac{\delta}{10^3} \right] \text{ MeV}. \quad (17)$$

It yields $\langle E_\gamma \rangle \simeq 0.23 \text{ MeV}$ for $\delta \simeq 10^3$ and $z=1$ –the mean redshift of the GRBs listed in Table I–, in good agreement with that measured in GRBs (Preece 2000).

For $n = 4$ the temperature decrease approximately as $1/t$. For $n > 4$ it diminishes faster than $1/t$ and for $n = 8$ it decreases faster than $1/t^2$, the ‘‘faster’’ being due, in both cases, to the effect of a decreasing $\gamma(t)$. For $T \sim 1/t^2$ behaviour, the pulse width narrows with time like $\sim E^{-0.5}$ in agreement with the analysis of Fenimore et al. (1995) who found, from a large sample of GRB pulses, that it narrows like $t \propto E^{-0.46}$.

The total radiated energy, in the CB rest frame, is roughly the thermal energy deposition within one radiation length from its front surface. After attenuation in the SN shell, it reduces to:

$$E_{\text{pulse}}^{\text{rest}} \approx \frac{\sigma_{\text{in}}(\text{pp}) \pi [R_{\text{CB}}^{t_p}]^2 \bar{X}_\gamma m_p c^2 \gamma(t)}{3 X_{\gamma_e} \sigma_T^2}, \quad (18)$$

where \bar{X}_γ is the radiation length in the obscuring shell averaged over the black body spectrum. For a typical γ -ray peak energy of $E_p \sim 1 \text{ MeV}$ in the SN rest frame, $\bar{X}_\gamma \simeq 10 \text{ g cm}^{-2}$. Consequently, the CB's radius at transparency

is $R_{\text{CB}}^{\text{tp}} = 4 \times 10^{11}$ cm and $E_{\text{pulse}}^{\text{rest}} \sim 3 \times 10^{45}$ erg, for $\gamma(t) \sim 10^3$.

This is consistent with the estimated GRB energies in Table I provided that the typical Doppler factors of GRBs are in the range $300 \leq \delta \leq 1000$.

4. Some simplifications and approximate predictions

A CB, in its rest system, is subject to a flux of high energy nuclei and electrons. While the electrons are being thermalized, they contribute a nonthermal high-energy tail of photons emitted via the “free-free” process. Such a power-law tail in an otherwise approximately-thermal emission is observed from young supernova remnants (see, e.g., Dyer et al. 2000) and clusters of galaxies (e.g., Fusco-Femiano et al. 1999; Rephaeli et al., 1999; Fusco-Femiano et al., 2000), both of which are systems wherein a dilute plasma at a temperature of $\mathcal{O}(1$ keV) is exposed to a flux of high energy cosmic rays. Thus, the CB emission can be modeled as a black body spectrum with a nonthermal power-law tail. If, for the sake simplicity, the energy spectrum of the surface radiation from a CB is approximated by a thermal black body radiation then, Eqs. (15–16) yield ,

$$\frac{dN}{dE dt} \propto \frac{(E t)^2}{\text{Exp}\{E t/H\} - 1} \text{Exp} \left\{ -[t_{\text{tp}}/t]^{n-1} \right\} \Theta[t]. \quad (19)$$

The total photon intensity and energy flux are, in this approximation:

$$\frac{dN}{dt} \propto \Theta[t] \frac{t_{\text{tp}}}{t} \text{Exp} \left\{ -[t_{\text{tp}}/t]^{n-1} \right\}, \quad (20)$$

$$F_E(t) \propto \Theta[t] \left[\frac{t_{\text{tp}}}{t} \right]^2 \text{Exp} \left\{ -[t_{\text{tp}}/t]^{n-1} \right\}. \quad (21)$$

Let the peak γ -ray energy at a fixed time during a GRB pulse be defined as $E_p^\gamma(t) \equiv \max [E^2 dI_\gamma/dE dt]$. Its value is $E_p^\gamma(t) \simeq 3.92 \delta T[t]/(1+z)$, so that, for t near or after t_{tp} :

$$E_p^\gamma(t) \simeq E_p^\gamma(t_{\text{tp}}) \Theta[t] \frac{t_{\text{tp}}}{t}. \quad (22)$$

The total “isotropic” energy of a GRB pulse – inferred from its observed fluence assuming an isotropic emission– can be deduced from Eq. (7), to be:

$$E_{\text{iso}} = \frac{4 \pi D_L^2 F}{1+z} \simeq E_{\text{pulse}}^{\text{rest}} \delta^3. \quad (23)$$

If CBs were “standard candles” with fixed mass, energy and velocity of expansion, and if all SN shells had the same mass, radius and density distribution, all differences between GRB pulses would result from their different distances and angles of observation. For such standard candles it follows from Eqs.(4-6,20, 21) that the observed durations (half widths at half maximum) of the photon intensity and of the energy flux density (Δt_I and Δt_F),

their peak values (N_p and F_p), and the peak energy (E_p^γ) in a single GRB pulse are roughly correlated to the total “observed” isotropic energy (E_{iso}) as follows:

$$\Delta t_I \propto (1+z) [E_{\text{iso}}]^{-1/3}, \quad (24)$$

$$\Delta t_F \propto (1+z) [E_{\text{iso}}]^{-1/3}, \quad (25)$$

$$N_p \propto E_{\text{iso}}, \quad (26)$$

$$F_p \propto [E_{\text{iso}}]^{4/3} (1+z)^{-1}, \quad (27)$$

$$E_p^\gamma \propto [E_{\text{iso}}]^{1/3} (1+z)^{-1}. \quad (28)$$

These approximate correlations can be tested using the sample of 15 GRBs with known redshifts. Because of the strong dependence of the CB pulses on the Doppler factor and their much weaker dependence on the other parameters, they may be approximately satisfied (see, e.g. Plaga 2000) in spite of the fact that CBs and SN shells are likely to be sufficiently varied not to result in standard candles.

5. Predictions of the Cannonball Model

Some common properties of GRB pulses (for detailed light curves see Kippen 2000; Mallozzi 2000) are observed to be:

- (a) The GRB fluences, integrated in energy and time, lie within one or two orders of magnitude above or below 10^{-5} erg/cm² (see, e.g., Paciesas et al. 1999).
- (b) Individual pulses are narrower in time, the higher the energy interval of their individual photons (see, e.g., Fenimore et al. 1995).
- (c) Individual pulses rise and peak at earlier time, the higher the energy interval of their individual photons (see, e.g., Norris et al. 1999; Wu and Fenimore 2000)
- (d) Individual pulses have smaller photon energies, the later the time-interval of observation (see, e.g., Preece et al. 1998) .
- (e) The energy spectrum of GRBs, or of their individual pulses, if plotted as $E^2 dN/dE$, rises with energy as E^α , with $\alpha \sim 1$, has a broad peak at $E \sim 0.1$ to 1 MeV, and decreases thereafter (see, e.g., Preece et al. 2000).
- (f) Most GRBs consist of pulses whose time-behaviour is a fast rise followed by an approximately exponential decay: a “FRED” shape. Some GRBs have non-FRED, roughly time-symmetric pulses (see e.g., Fenimore et al. 1995 and references therein) The overwhelming majority of GRBs are either made of FRED or non-FRED pulses: there are no GRBs with mixed pulse-shapes.

All of the above items are properties of the CB model, as was shown in Dar and De Rújula 2000b. Figs. 2-4, taken from this reference, demonstrate the success of the CB model in explaining the temporal structure of GRBs, the spectrum of individual pulses and their temporal evolution.

6. GRB afterglows

Far from their parent SNe, the CBs are slowed down by the interstellar medium (ISM) they sweep, which has been previously ionized by the forward-beamed CB radiation (traveling essentially at $v = c$, the CB is “catching up” with this radiation, so that the ISM has no time to recombine). As in the jets and lobes of quasars, a fraction of the swept-up ionized particles are “Fermi accelerated” to cosmic-ray energies and confined to the CB by its turbulent magnetic field, maintained by the same confined cosmic rays (Dar and Plaga 1999). The bremsstrahlung and synchrotron emissions from the high energy electrons in the CB, boosted by its relativistic bulk motion, produce afterglows in all bands between radio and X-rays, collimated within an angle $\sim 1/\gamma(t)$, that widens as the ISM decelerates the CB.

A CB of roughly constant cross section, moving in a previously ionised ISM of roughly constant density, slows down according to $d\gamma/dx = -\gamma^2/x_0$, with $x_0 = M_{\text{CB}}/(\pi R_{\text{CB}}^2 n m_p)$ and n the number density along the CB trajectory. For $\gamma^2 \gg 1$, the relation between the length of travel dx and the (red-shifted, relativistically aberrant) time of an observer at a small angle θ is $dx = [2c\gamma^2/(1 + \theta^2\gamma^2)] [dt/(1+z)]$. Inserting this into $d\gamma/dx$ and integrating, one obtains:

$$\frac{1 + 3\theta^2\gamma^2}{3\gamma^3} = \frac{1 + 3\theta^2\gamma_0^2}{3\gamma_0^3} + \frac{2ct}{(1+z)x_0}, \quad (29)$$

where γ_0 is the Lorentz factor of the CB as it exits the SN shell. The real root $\gamma = \gamma(t)$ of the cubic Eq. (29) describes the CB slowdown with observer’s time.

The radiation emitted by a CB in its rest system (bremsstrahlung, synchrotron, Compton-boosted self-synchrotron), is boosted and collimated by the CB’s motion, and its time-dependence is modified by the observer’s time flowing $(1+z)/\delta$ times faster than in the CB’s rest system. For $\gamma \gg 1$, an observer at small θ sees an energy flux density:

$$F[\nu] \sim \delta^3 F_0(\nu [1+z]/\delta) A(\nu, z), \quad (30)$$

where $F_0(\nu_0)$ is the CB emission in its rest frame, $\delta(t)$ is given by Eq. (5) with $\gamma = \gamma(t)$ as in Eqs. (29), and $A(\nu, z)$ an eventual absorption dimming.

Neglecting energy deposition through collision of the CB with the ISM during the afterglow regime and energy losses due to expansion and radiation, the CB’s afterglow is dominated by a steady electron synchrotron radiation from the magnetic field in the CB (valid only for slowly expanding/cooling CBs in a low density ISM and for frequencies where the attenuation length due to electron free-free transitions exceeds its radius). The spectral shape of synchrotron emission in the CB rest frame is $F_0 \sim \nu_0^{-\alpha}$, with $\alpha = (p-1)/2$ and p the spectral index of the electrons. For equilibrium between Fermi acceleration and synchrotron and Compton cooling, $p \approx 3.2$ and

$\alpha \approx 1.1$, while for small cooling rates, $p \approx 2.2$ and $\alpha \approx 0.6$ (Dar and De Rújula 2000c), or $p \approx 1.2$ and $\alpha \approx 0.1$ if Coulomb losses dominate. At very low radio frequencies self-absorption becomes important and $\alpha \approx -1/3$ (2.1) for optically thin (thick) CBs.

Since $\gamma(t)$, as in Eq. (29), is a decreasing function of time, the afterglow described by Eq. (30) may have a very interesting behaviour. An observer may initially be outside the beaming cone: $\theta^2\gamma^2 > 1$, as we shall argue to be the case for GRB 980425, for which we estimate $\gamma_0^2\theta^2 \sim 200$ (other relatively dim GRBs in Table I, such as 970228 and 970508, may also be of this type). The observed afterglow would then initially rise with time. As γ decreases, the cone broadens, and around $t = t_p$ when $\gamma\theta \sim 1$ (when the observer enters the ‘beaming cone’ of the CB) the afterglow peaks and then begins to decline. Beyond the peak, when $\gamma^2\theta^2 \gg 1$ and where $\gamma \sim t^{-1/3}$, the afterglow declines like

$$F[\nu] \sim F[\nu, t_p] \left[\frac{(t_p/t)^{1/3}}{1 + (t_p/t)^{2/3}} \right]^{3+\alpha+\beta} A(\nu, z), \quad (31)$$

where $F_0 \sim \nu^{-\alpha} t^{-\beta}$ in the CB rest frame. For steady emission, i.e., for small emission and energy deposition rates, $\beta = 0$. For an emission rate which is in equilibrium with the energy deposition rate in the CB rest frame by the incident ISM particles (that is proportional to γ^2), $\beta = 2/3$. Eq. (31) describes well the late afterglows of most GRBs, including their radio afterglows (if one correct it for absorption in the CB and along the line of sight).

This is demonstrated in Fig. 5 for GRB 000418 where its late afterglow in the R band as predicted by Eqs.(29,31) is compared with the observations that were compiled in Klose et al. 2000. The normalization and t_p were adjusted to fit the data. A contribution from a SN1998bw-like SN placed at the GRB redshift, $z=1.11854$, as in Eq.(1) with Galactic extinction $A_R = 0.09$ magnitudes was added to the CB light curve.

Eqs. (29,30) may explain the puzzling initial rise of the optical afterglow of GRBs 970228 and 970508, as well as the second peak around $t_p \sim 3-4 \times 10^6$ s in the unresolved radio emission from SN1998bw/GRB 980425 (Kulkarni et al. 1998a; Frail et al. 1999), if it corresponds to the GRBs afterglow. This is demonstrated in Fig. 6. where the afterglow of GRB 970508 in the R band is compared with Eqs. (29,30), for the measured index $\alpha = 1.1$. The adjusted parameters are the height, the time of the afterglow’s peak and the product $\theta\gamma_0$. The figure is for a single CB; with a few of them at chosen times and relative fluxes, it would be easy to explain the early “warning shots” at $t < 1$ day and the abrupt rise at $t = 1$ to 2 days. At $t \gg t_p$, however, they would add up to a single curve like the one shown in the figure.

When the CB enters the Sedov–Taylor phase its radius increases as $t^{2/5}$. The Lorentz factor of electrons decreases like $t^{-6/5}$. In equipartition, the magnetic field decreases like $t^{-3/5}$. Wijers et al. (1997) have shown that these facts

lead to an afterglow decline $F_\nu \sim t^{-(15\alpha-3)/5} \sim t^{-2.7}$ for $\alpha \sim 1.1$ CB at rest, as was observed for the late-time afterglows of some GRBs. Note, however, that if the CB enters the Sedov-Taylor phase in flight, Eq. (30) predicts $F_\nu \sim t^{-(50\alpha+6)/15}$, i.e., $F_\nu \sim t^{-2.4}$ for $\alpha \sim 0.6$ which changes to $F_\nu \sim t^{-4}$ for $\alpha \sim 1.1$.

7. GRB 980425: a special case

In the list of Table I, GRB 980425 stands out in two — apparently contradictory— ways: it is, by far, the closest ($z = 0.0085$, $D_L = 39$ Mpc) and it has, by far, the smallest implied spherical energy: 8.1×10^{47} erg, 4 to 6 orders of magnitude smaller than that of other GRBs. However, if GRB 980425 was not abnormal, Eq. (23) tells us that the peculiarities of GRB 980425 can be understood if its source was “fired” from SN1998bw with a bulk-motion Lorentz factor $\gamma \sim 1000$, at an angle $\theta \approx 15/\gamma$ relative to our line of sight. Then, for $\theta \ll 1$ and $\gamma \gg 1$, its projected sky velocity

$$v_T^+ \approx \frac{2\gamma^2\theta}{(1+\gamma^2\theta^2)} c, \quad (32)$$

yields superluminal velocities (Rees 1966) $v_T \approx 2c/\theta$ for $\gamma^2\theta^2 \gg 1$, and $v_T \approx 2c\gamma^2\theta$, for $\gamma^2\theta^2 \ll 1$, provided $2\gamma^2\theta > 1$. Its transverse superluminal displacement, D_T , from the SN position can be obtained by time-integrating v_T , as in Eq. (32), using $\gamma(t)$ as in Eq. (29). The result can be reproduced, to better than 10% accuracy, by using the approximation $v_T \sim 2\gamma^2\theta c$, valid for $\gamma < 1/\theta$ (or $t > t_p$, the afterglow’s peakttime):

$$D_T \simeq \frac{2c t_p}{\theta} \left[\frac{t}{t_p} \right]^{1/3}. \quad (33)$$

At present ($t \sim 850$ d), the displacement of the GRB from the initial SN/GRB position is $D_T \sim 20(\gamma_0/10^3)$ pc, corresponding to an angular displacement $\Delta\alpha \sim 100(\gamma_0/10^3)$ mas, for $z = 0.0085$, $t_p \sim 3.5 \times 10^6$ s.

The two sources, now a few tens of mas away, may still be resolved by HST. In Fig. 7 we show our prediction for the late-time V-band light curve of SN1998bw/GRB 980425. The SN curve is a fit by Sollerman et al. (2000) for energy deposition by ^{56}Co decay in an optically thin SN shell. The GRB light curve is our predicted afterglow for GRB 980425, as given by Eqs. (29,30), and constrained to peak at the position of the second peak in the radio observations (Kulkarni et al. 1998a; Frail et al. 1999). The fitted normalization is approximately that of the mean afterglow of the GRBs in Table I, suppressed by the same factor as its γ -ray fluence relative to the mean γ -ray fluence in Table I. The joint system has at present (day ~ 850) an extrapolated magnitude $V \sim 26$ (Fynbo et al. 2000). It can still be resolved from its host galaxy ESO-184-G82 by HST and, perhaps, by VLT in good seeing conditions. An extrapolation of the V-band late time curve of SN1998bw

(Sollerman et al. 2000) suggests that the present magnitude of the SN is $V \sim 28$, which is near the detection limit of HST and is dimming much faster than ^{56}Co -decay would imply.

In the GHz radio band, the system has been last observed in February 1999 by ATCA (Australia’s Telescope Compact Array) to have an $\mathcal{O}(1)$ mJy flux density (Frail et al. 2000) and to have approached a power-law time decline with a power-law index -1.47 . If a Sedov-Taylor break in the radio afterglow of GRB 980425 has not occurred yet, its spectral density may still be strong enough to determine its position with ATCA and VLBI to better than mas precision. If the second peak is the GRB’s afterglow, the two radio centroids should now be separated by $\sim \gamma_0/10$ mas (or by $\sim \gamma_0/20$ mas, if the first peak is the afterglow). A refined location from a reanalysis of the early ATCA observations (Kulkarni et al 1998a; Frail et al. 1999) of the initial SN and of the late afterglow may also reveal a superluminal displacement.

If the GRB afterglow has entered the late fast-decline phase seen in some GRB afterglows and in quasar and microquasar “afterglows” from jetted ejections (observed power-law index -2.7 ± 0.3), a further delay in follow-up observations can make it very difficult or impossible to detect and resolve the GRB/SNR radio image into its two predicted images.

A GRB as close as GRB 980425 ($z = 0.0085$) should occur only once every ~ 10 years and its associated supernova may be only occasionally observed. For typical GRBs ($z \sim 1$) there is no hope of resolving them with HST into two separate SN and GRB images. Resolving them with VLBI would also be arduous. For these reasons, we exhort interested observers to consider immediate high-resolution optical (STIS) and radio (ATCA and VLBI) follow-up observations of SN1998bw and the afterglow of GRB980425.

8. X-ray lines in GRB afterglows

Lines in the X-ray afterglow of GRBs have been detected in four GRBs (GRB 970508, Piro et al. 1999; GRB 970828, Yoshida et al 1999; GRB 991216, Piro et al. 2000; GRB 000214, Antonelli et al. 2000). Their energies are listed in Table II. They were interpreted as iron lines emitted from a large mass of iron that was photoionized by the GRB. However, this interpretation raises many questions (see, e.g., Vietri 2000).

8.1. Origin of the X-ray lines

The CB model offers an alternative interpretation for the origin of the X-ray lines in the “early” GRB afterglow - hydrogen recombination lines which are Doppler shifted to X-ray energies by the CB relativistic motion:

As long as the CB is opaque to its internal radiation, it expands with the relativistic speed of sound, $c\sqrt{3}$ in

its rest frame, and cools with $T_{\text{CB}} \sim 1/R_{\text{CB}} \sim 1/t$. When $R_{\text{CB}} \simeq [3 M_{\text{CB}} \sigma_{\text{T}} / (4 \pi m_{\text{p}})]^{1/2}$, where $\sigma_{\text{T}} \simeq 0.65 \times 10^{-24} \text{ cm}^2$ is the Thomson cross section, it becomes optically thin and its internal radiation escapes. This end to the CB's γ -ray pulse takes place at $t \simeq R_{\text{CB}} / \sqrt{3} c \delta \simeq 2 \times (10^3 / \delta) \text{ s}$ in the observer frame. Due to the escape of its internal radiation, its internal pressure drops and its expansion rate is slowed down by sweeping up the ISM. During this phase it cools mainly by emission of bremsstrahlung and synchrotron radiation. Its ionization state is described by the Saha equation

$$\frac{x^2}{1-x} = \frac{(2 \pi m_{\text{e}} c^2 k T)^{3/2}}{n h^3 c^3} e^{-\chi/k T} \quad (34)$$

with $x = n_{\text{e}}/n$, n being the the baryon density in the shell, $\chi = 13.6 \text{ eV}$ is the hydrogen binding energy T is the plasma temperature in K and n_{e} is the density of free electrons in cm^{-3} . When the electron temperature in the CB approaches 5000 K, electrons begin to recombine with protons into hydrogen. The exponential term in the Saha equation confines this recombination phase of the CB to a temperature around 4500K (for CBs with $10^5 \text{ cm}^{-3} < n_{\text{e}} < 10^6 \text{ cm}^{-3}$, as we shall estimate later). The recombination produces strong emission of Ly_{α} line (and, perhaps, a recombination edge above the Ly_{∞} line) which is Doppler shifted by the CB motion to X-ray energy in the observer frame:

$$E_{\alpha} \simeq \frac{10.2}{(1+z)} \left[\frac{10^3}{\delta} \right] \text{ keV}, \quad (35)$$

$$E_{\text{edge}} \simeq \frac{13.6}{(1+z)} \left[\frac{10^3}{\delta} \right] \text{ keV}. \quad (36)$$

The total number of these recombination photons is approximately equal to the baryonic number of the CB, $N_{\text{b}} \simeq E_{\text{CB}}/m_{\text{p}} c^2 \gamma(0) \simeq 6.7 \times 10^{51} (E_{\text{CB}}/10^{52} \text{ erg}) (10^3/\gamma(0))$. Thus, the photon fluence of these lines (line-fluence) at a luminosity distance D_{L} is

$$N_{\text{lines}} \simeq N_{\text{b}} \frac{(1+z)^2 \delta^2}{4 \pi D_{\text{L}}^2}. \quad (37)$$

The measured energies of the observed X-ray lines in the above 4 GRBs and the Doppler factors implied by their interpretation as hydrogen recombination features are listed in Table II. The inferred Doppler factors are consistent with those needed in the CB model ($\delta \sim 10^3$) to explain the intensity and duration of the GRB pulses.

Note that the 4.4 keV line in the afterglow of GRB 991216 may be either a hydrogen recombination edge from the same CB that produces the 3.49 keV line, or a $\text{Ly} - \alpha$ line from another CB.

8.2. Observational Tests

There are various independent tests of the interpretation of the X-ray lines as hydrogen recombination features that are Doppler shifted to X-ray energies by the CB motion:

a. Time and duration of line emission: The mean time for radiative recombination in hydrogenic plasma is $r_{\text{rec}} \approx 3 \times 10^{10} T^{-1/2} n_{\text{e}} \text{ s}^{-1}$. In the observer frame this recombination time is

$$\Delta t_{\text{L}} \approx \frac{3 \times 10^{10} (1+z) T^{1/2}}{n_{\text{e}} \delta} \text{ s}. \quad (38)$$

The emission rate of bremsstrahlung by an hydrogenic plasma is $L \simeq 1.43 \times 10^{-27} n_{\text{e}}^2 T^{1/2} \text{ erg cm}^{-3} \text{ s}^{-1}$, and the cooling time of the CB to temperature T in the observer frame is

$$t_{\text{brem}} \simeq \frac{2.9 \times 10^{11} (1+z) T^{1/2}}{n_{\text{e}} \delta} \text{ s}. \quad (39)$$

Thus, the ratio $\Delta t_{\text{L}}/t_{\text{brem}} \simeq 0.10$, where the dependence on Doppler factor, electron density, temperature and redshift of the CB has been canceled out, is a universal ratio for CB afterglows, independent of their detailed properties. This prediction is consistent with the observations of the X-ray line in GRB 980828 where $\Delta t_{\text{L}}/t_{\text{brem}} \simeq 0.05$ with a large (\sim factor 2) uncertainty (Yoshida et al. 1999).

However, the above estimate is valid only for a single CB (originally ejected, or one that was formed by overtaking and merger of separately ejected CBs). Generally, the afterglows of different CBs cannot be resolved either spatially or temporally. Their individual afterglows are blended into a single afterglow. Because of their different Lorentz and Doppler factors, X-ray line emission may extend over a much longer time, $\Delta t_{\text{L}} \simeq t_{\text{brem}}$. This may be the case in the observations of X-ray line emission during the afterglow of GRB 970508 and GRB 000214 by BeppoSAX and of GRB 991216 by Chandra which were too short both in time and of statistics to measure accurately enough the duration of the line emission.

b. Photon fluences : Table II also reports the total photon fluence in X-ray lines during the observation time and the total baryon number required to produce the lines as predicted by Eq. (37). These baryon numbers are within the range expected for SNe CBs/jets ($N_{\text{b}} \simeq 6.5 \times 10^{51 \pm 1}$). However, because the observation times may not have extended over the full time of line emission, these baryon numbers may underestimate the baryon number of the CB/jet.

c. Line width : Thermal broadening of both the recombination lines and the recombination edge are rather small. However, the Doppler factors of the CBs decrease with time during the line emission because of the decrease of their Lorentz factors due to their deceleration by the ISM. At late time, $\gamma \sim t^{-1/3}$, for a single CB and as a result the line energy shifts by $\Delta E_{\text{L}} \simeq (\Delta t_{\text{L}}/3 t_{\text{brem}}) E_{\text{L}} \simeq 0.04 E_{\text{L}}$ during the line emission. The decrease in the line energy with time during the line emission is a clear fingerprint of the origin of the lines. When integrated over time (in order to increase statistics) the line shift will appear as a line broadening. The above estimate of this line broadening is consistent with the reported widths of the X-ray lines.

d. The CB radius during line emission: The electron density in the CB during the line emission can be inferred from the observed time and duration of the line emission, using Eqs. (38),(39). Then, the CB radius can be estimated from the total baryon number which is inferred from the measured line-fluence. This radius estimate is not sensitive to the accuracy of the observations since it depends on the third root of N_b/n_e . The three GRBs with measured redshifts yield $R_{CB} \sim (1 - 2) \times 10^{15}$ cm for $t \sim 1 - 2$ days in the observer frame. If a CB continues to expand within the first few weeks with the same mean speed of expansion as in the first day or two, its radius after a month reaches $\simeq (3 - 6) \times 10^{16}$ cm (only then the swept up ISM mass begins to be comparable to the CB mass). Indeed, from VLA observations of scintillations (Goodman 1997) in the radio afterglow of GRB 970508 and their disappearance after a month it was inferred (Taylor et al. 1997) that the linear size of its source a month after burst was $\approx 10^{17}$ cm, i.e., corresponding to $R_{CB} \sim 5 \times 10^{16}$ cm.

9. Conclusions

GRBs and their afterglows may be produced by jets of extremely relativistic cannonballs in SN explosions. The cannonballs which exit the supernova shell/ejecta reheated by their collision with it, emit highly forward-collimated radiation which is Doppler shifted to γ -ray energy. Each cannonball corresponds to an individual pulse in a GRB. They decelerate by sweeping up the ionised interstellar matter in front of them, part of which is accelerated to cosmic-ray energies and emits synchrotron radiation: the afterglow. When the cannonballs cool below 4500K, electron-proton recombination to hydrogen produces Ly- α emission which is Doppler shifted to X-ray energy.

The Cannonball Model cannot predict the timing sequence of the GRB pulses, it fares very well in describing the total energy, energy spectrum, and time-dependence of the individual γ -ray pulses and their afterglow and explains the X-ray lines observed in some GRB afterglows.

For the GRB to be observable, the CBs must be close to the line of sight, implying that their afterglows would appear to move superluminally. Only one of the located GRBs (980425) is close enough to us for this superluminal displacement to be observable with the currently available resolution. Its afterglow may by now be too dim to be seen. Or it may not. If observed, the superluminal displacement of this GRB's afterglow would be a decisive card in favour of cannonballs, as opposed to stationary fireballs.

The Cannonball model predicts that GRB pulses are accompanied by short pulses of TeV neutrinos and sub TeV γ -rays, which begin and peak a little earlier and are much more energetic than the GRB pulses. These high energy emission should be visible in ground based (sub TeV photon) and underground (neutrino) telescopes.

There are other events in which a variety of GRBs could be produced by the CB mechanism: large mass accretion episodes in binaries including a compact object, mergers of neutron stars with neutron stars or black holes (Paczynski 1986, Goodman et al. 1987), transitions of neutron stars to hyperon- or quark-stars (Dar 1999; Dar and De Rújula, 2000d), etc. In each case, the ejected cannonballs would make GRBs by hitting stellar winds or envelopes, circumstellar mass or light. I discussed only core-collapse SN explosions, as the GRBs they would produce, although relatively "standard", satisfactorily reproduce the general properties of the heterogeneous ensemble of GRBs, their afterglows and even their X-ray line emission.

Acknowledgements: The material presented in this talk is based on work done in collaboration with Alvaro De Rújula. The research was supported in part by the Fund for Promotion of Research at the Technion and by the Hellen Asher Fund for Space Research.

References

- Antonelli, L.A., et al., 2000, astro-ph/0010221 to be published
- Belloni T., et al., 1997, ApJ 479, 145
- Bloom J.S., et al., 1999, Nature 401, 452
- Cen R., 1999, ApJ 524, 51
- Celotti A., et al. 1997 MNRAS 286, 415
- Costa E., et al., 1997, Nature 387, 783
- Dar A., 1998, ApJ 500, L93
- Dar A., 1999a, A&AS 138, 505
- Dar A., 1999b, GCN Report No. 346
- Dar A., De Rújula, A., 2000a, astro-ph/0008474 (A&A)
- Dar A., De Rújula, A., 2000b, astro-ph/0012227 (A&A)
- Dar A., De Rújula, A., 2000c, astro-ph/0005080 (MNRAS)
- Dar A., De Rújula, A., 2000d, astro-ph/0002014 (MNRAS)
- Dar A., Plaga R., 1999, A&A 349, 259
- De Rújula A., 1987, Phys. Lett. 193, 514
- Dyer K.K., et al., 2000, astro-ph/0011578
- Fassia A., et al., 2000, astro-ph/0011340
- Fenimore E.E., et al., 1995, ApJ 448, L101
- Frail D.A., et al., 1999, <http://www.narrabri.atnf.csiro.au/public/grb980425/>
- Fruchter A.S., et al., 1999, astro-ph/9903236
- Fruchter A.S., et al., 2000, GCN 627
- Fusco-Femiano R., et al., 1999, ApJ, 513, L21
- Fusco-Femiano R., et al., 2000, astro-ph/0003141
- Fynbo J.U., et al., 2000, astro-ph/0009014
- Galama T.J., et al., 1998, Nature 395, 670
- Galama T.J., et al., 2000, ApJ 536 185
- Ghisellini G., 2000, astro-ph/0012125
- Goodman J., Dar, A., Nussinov, S., 1987, ApJ 314, L7
- Goodman J., 1997, NA 2, 449
- Groom D.E., et al., 2000, *Review of Particle Physics*, Eur. Phys. J. C15, 1
- Hjorth J., et al., 1999, GCN 403
- Hjorth J., et al., 2000, ApJ 534, 147L
- Holland S., et al., 2000, submitted
- Iwamoto K., et al., 1998, Nature 395, 672
- Kippen R.M., et al., 1998, GCN 67
- Kippen R.M., 2000, http://www.batse.msfc.nasa.gov/~kippen/batserbr/brbr_obs.html

Klose S., et al., 2000, astro-ph/0007201
 Kotani T., et al., 1996, PASPJ 48, 619
 Kulkarni S.R., et al., 1998a, Nature 395, 663
 Kulkarni S.R., et al., 1998b, Nature 393, 35
 Kulkarni S. et al., 1999a, Nature, 398, 389
 Lazatti D, et al. MNRAS, 304, L31
 Lyne A.G., Lorimer, D.R., 1994, Nature 369, 127
 MacFadyen A.I., Woosley S.E., 1999, ApJ 524, 168
 MacFadyen, A.I., Woosley S.E., Heger A., 1999, astro-ph/9910034
 Madau P., 1998, astro-ph/9801005
 Malozzi, R.S., 2000, <http://www.batse.msfc.nasa.gov/batse/>
 Margon B.A., 1984, ARA&A 22, 507
 Meszaros P., Rees M.J., 1992, MNRAS 257, 29
 Metzger M.R., et al., 1997, Nature 387, 878
 Mirabel I.F., Rodriguez, L.F., 1994, Nature 371, 46
 Mirabel, I.F., Rodriguez, L.F., 1999a, ARA&A 37, 409
 Mirabel, I.F., Rodriguez, L.F. 1999b, astro-ph/9902062
 Norris J.P., et al., 1999, astro-ph/9903233
 Nakamura T. et al., 2000, astro-ph/0007010
 Paciesas W.S., et al., 1999, ApJS 122, 465
 Paczynski B., 1986, ApJ 308, L43
 Paczynski B., 1998, ApJ 494, L45
 Pian E., et al., 1999, A&A 138(3), 463
 Piro L., et al., 1999, ApJ, 514, L73
 Piro L., et al., 2000, Science, 290, 955
 Plaga R., 2000, astro-ph/001206
 Preece R.D., et al., 1998, ApJ 496, 849
 Preece R.D., et al., 2000, ApJS 126, 19
 Rees M.J., 1966, Nature 211, 468
 Reichart D.E., 1999, ApJ 521, L111
 Rephaeli Y., et al., 1999, ApJ 511 L21
 Rodriguez L.F., Mirabel, I.F., 1999, ApJ 511, 398
 Salamanca, I., et al., 1998, MNRAS 300L, 17
 Sahu K.C., et al., 2000, ApJ 540, 74
 Shaviv N.J., Dar A., 1995, ApJ 447, 863
 Soffitta P., et al., 1998 IAU Circ. No. 6884
 Sollerman J., et al., 2000, astro-ph/0006406
 Sokolov V.V., et al., 2000, to be published
 Taylor G.J., et al., 1997, Nature 389, 263
 van den Bergh S. Tammann G.A., 1991, ARA&A 29, 363
 van Paradijs J., et al., 1988, A&A 192, L147
 Vietri M., et al., 1999, MNRAS, 308, L29
 Vietri M., 2000, astro-ph/0011580
 Wieringa M.H., et al., 1999, A&AS 138, 467
 Wijers R.A.M.J., Rees M.J., Meszaros P., 1997, MNRAS 288, L5
 Wilson A.S., et al., 2000, astro-ph/0008467
 Woosley, S.E. 1993, ApJ 405, 273
 Woosley, S.E., MacFadyen, A.I., 1999, A&AS 138, 499
 Woosley S.E., MacFadyen, A.I., 1999, A&AS 138, 499
 Wu B., Fenimore E., 2000, ApJ 535L, 29
 Yoshida A. et al., 1999, A&A, 138S, 433

Table I - Gamma ray bursts of known redshift z

GRB	z	D_L^a	F_γ^b	E_γ^c	M^d
970228	0.695	4.55	0.17	0.025	25.2
970508	0.835	5.70	0.31	0.066	25.7
970828	0.957	6.74	7.4	2.06	—
971214	3.418	32.0	1.1	3.06	25.6
980425	0.0085	0.039	0.44	8.14 E-6	14.3
980613	1.096	7.98	0.17	0.061	24.5
980703	0.966	6.82	3.7	1.05	22.8
990123	1.600	12.7	26.5	19.8	24.4
990510	1.619	12.9	2.3	1.75	28.5
990712	0.430	2.55	—	—	21.8
991208	0.706	4.64	10.0	1.51	>25
991216	1.020	7.30	25.6	8.07	24.5
000131	4.51	—	3.51	11.0	—
000301c	2.040	17.2	2.0	2.32	27.8
000418	1.119	8.18	1.3	0.49	23.9
000926	2.066	17.5	2.5	2.98	24

Comments: *a*: Luminosity distance in Gpc (for $\Omega_m = 0.3$, $\Omega_\Lambda = 0.7$ and $H_0 = 65 \text{ km s}^{-1} \text{ Mpc}^{-1}$). *b*: BATSE γ -ray fluences in units of $10^{-5} \text{ erg cm}^{-2}$. *c*: (Spherical) energy in units of 10^{53} ergs. *d*: R-magnitude of the host galaxy, except for GRB 990510, for which the V-magnitude is given.

Table II - GRB afterglows with X-ray lines

GRB	z	E_{line}	F_{line}	Δt_{obs}	δ_{line}	N_b
970508	0.835	3.4	1.5	30	612	3×10^{51}
970828	0.957	5.04	0.45	24	967	$> 7 \times 10^{50}$
991216	1.020	3.49	0.39	12	691	$> 1.3 \times 10^{51}$
991216	1.020	4.4	0.47	12	800	$> 1.3 \times 10^{51}$
000214	—	4.7	1.0	104	≥ 460	—

Comments: Line energies in keV. Observation times in ks. All lines were assumed to be a Doppler shifted $L\gamma-\alpha$ lines. The line fluences (in cm^{-2}) and the baryon numbers are lower limits because of partial observation times.

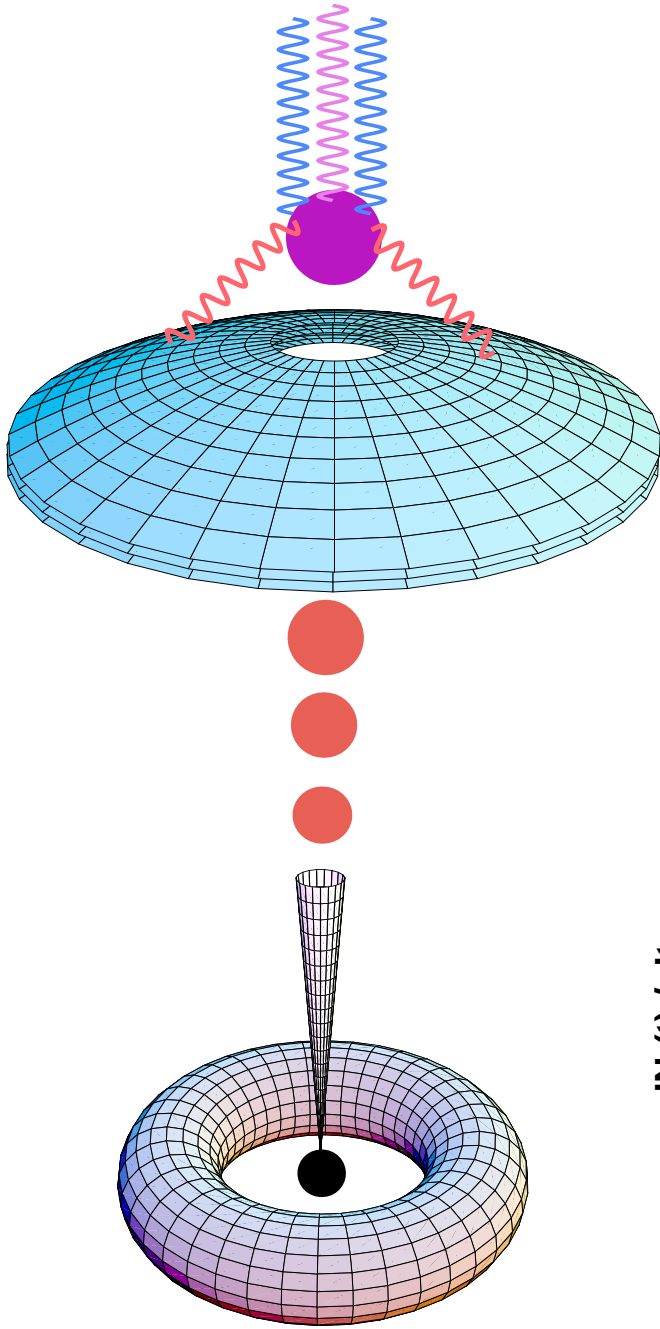


FIG. 1.— An “artist’s view” (not to scale) of the CB model of GRBs and their afterglows. A core-collapse SN results in a compact object and a fast-rotating torus of non-ejected fallen-back material. Matter accreting (and not shown) into the central object produces a narrowly collimated beam of CBs, of which only some of the “northern” ones are depicted. As these CBs pierce the SN shell, they heat and reemit photons. They also scatter light from the shell. Both emissions are Lorentz-boosted and collimated by the CBs’ relativistic motion.

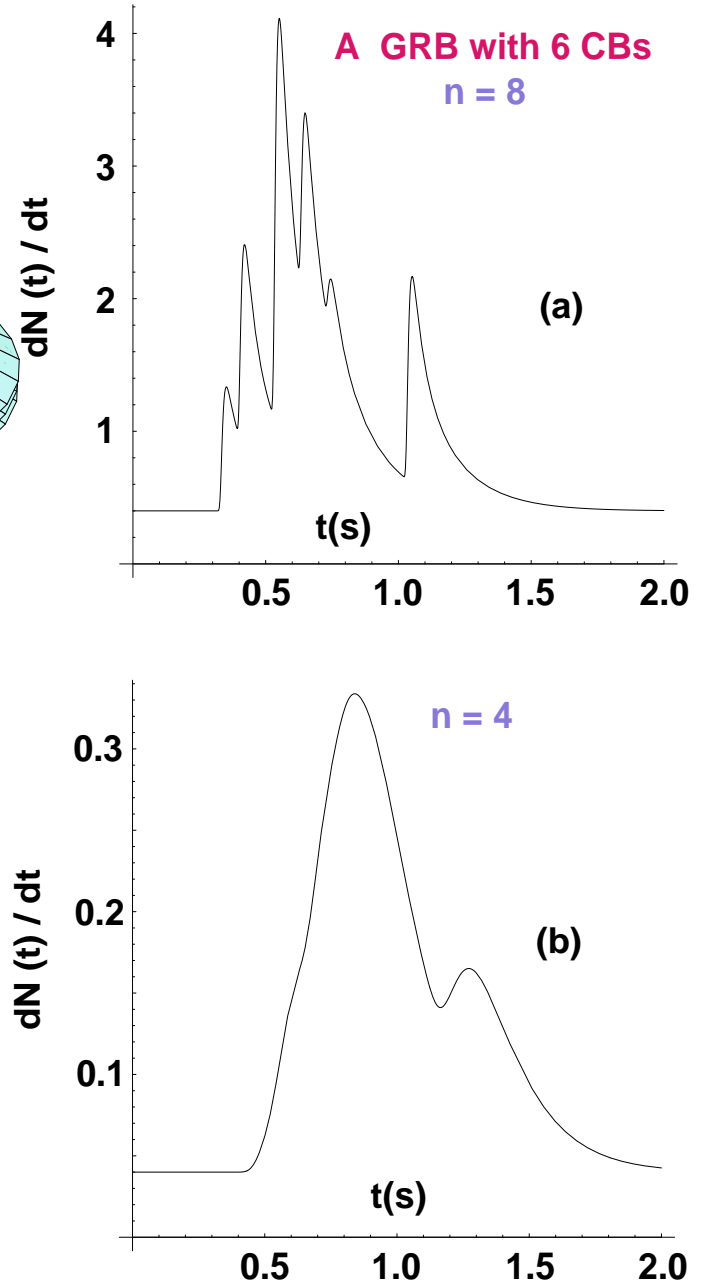


FIG. 2.— “Synthetic” GRB light curves, generated by shooting six CBs at random in a 1.5 s time-interval, and with random values of E_{CB} within a factor 2, taken from Dar and De Rújula 2000b. The only difference between (a) and (b) is that $n = 8$ in (a), while $n = 4$ in (b). All other parameters in this figure have their reference values. The figure illustrates how a CB produces a GRB pulse, but a GRB-pulse may not correspond to a single CB.

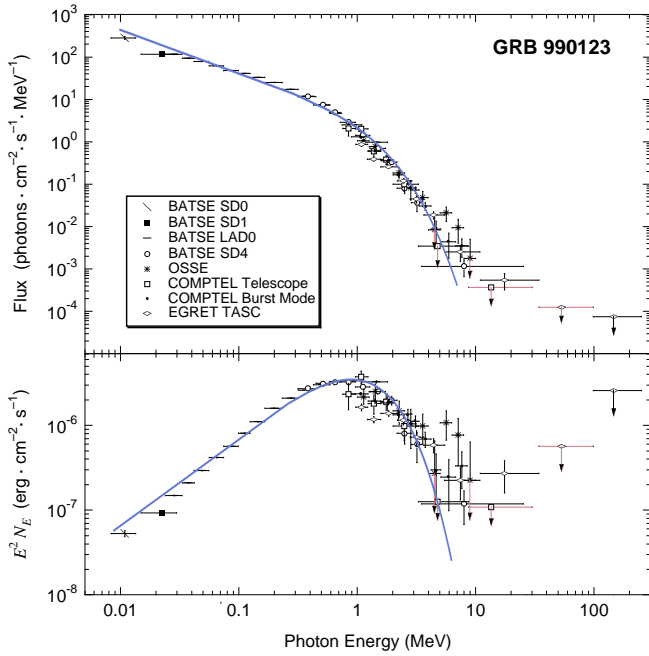


FIG. 3.— Comparison of theory and observation (taken from Dar and De Rújula 2000b) for the time-integrated energy distributions dN/dE and $E^2 dN/dE$, in the case of GRB 990123. Notice that many experimental points at the higher energies are only upper limits.

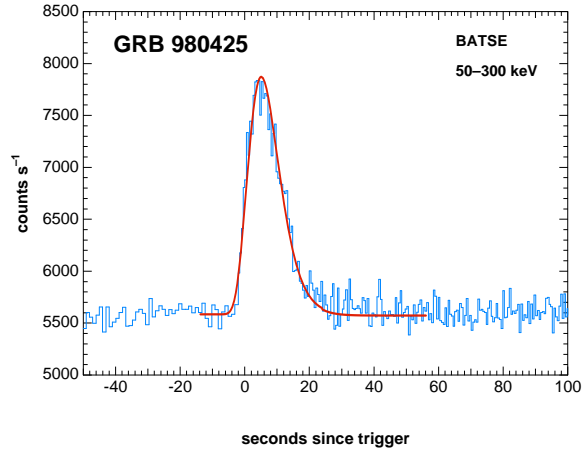


FIG. 4.— Comparison of theory and observation for the light curve of GRB 980425, in the 50-300 keV energy interval taken from Dar and De Rújula 2000b.

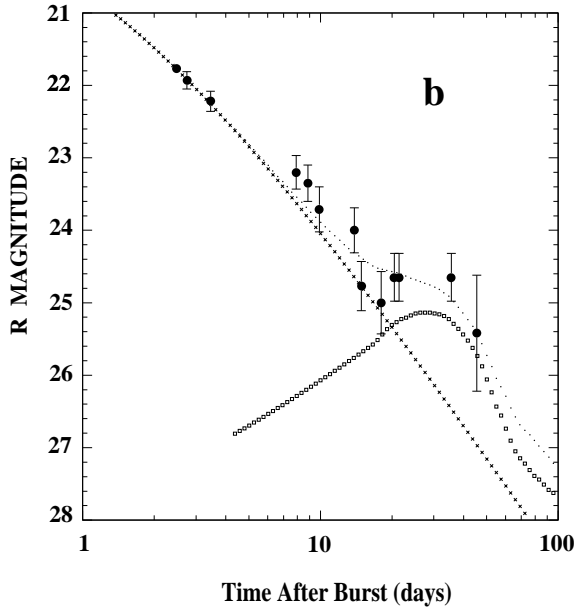
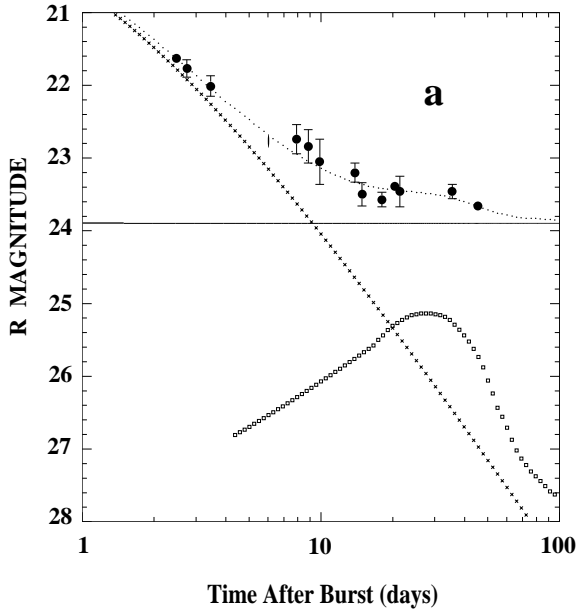


FIG. 5.— Comparisons between the R-band light curve for GRB 000418 (dotted lines) as calculated from the Cannonball model (Dar and De Rújula (2000a) and the observations as compiled by Klose et al. (2000). a) Without subtraction of the host galaxy’s contribution: the straight line with $R = 23.9$ (Fruchter et al. 2000). b) With the host galaxy subtracted. The CB’s afterglow is given by Eq.(29,30) with spectral index $\alpha = 1.9$ (Klose et al. 2000) and is indicated by crosses. The contribution from a SN1998bw-like SN placed at $z=1.11854$, as in Eq.(1) with Galactic extinction $A_R = 0.09$ magnitudes, is indicated by open squares. The dotted line is the sum of contributions. The SN bump is clearly discernible.

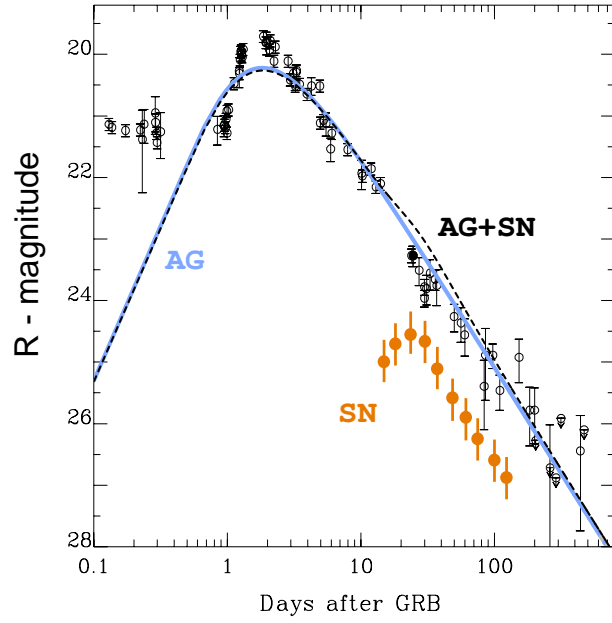


FIG. 6.— The R-band light curve of the afterglow of GRB 970508 as compiled by Fruchter et al. (1999) with a constant ($R = 25.2$ magnitude) host galaxy subtracted from all the measurements. The blue “AG” curve is given by Eqs. (29,30) (Dar and De Rújula 2000a). The contribution from a SN1998bw-like SN, placed at the GRB redshift $z = 0.835$, given by Eq.(1), is indicated (in red) and makes very little difference when added to the afterglow.

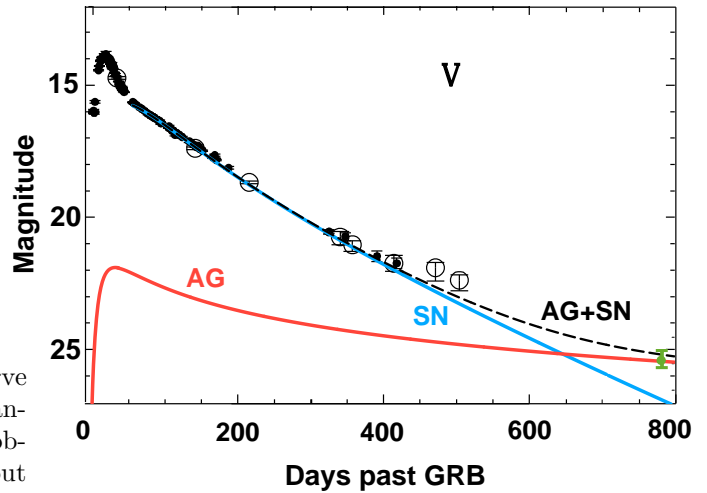


FIG. 7.— The V-band light curve of SN1998bw/GRB 980425, with the blue “SN” curve a fit to the SN by Sollerman et al. (2000). The red “AG” curve is the CB model prediction for the afterglow as given by Eqs. (29,30), fit to peak at the position of the observed second radio peak, and to reproduce the most recent observation at $d = 778$. (Dar and De Rújula 2000a). The dashed curve is the total.